



1 **Land-atmosphere interactions in sub-polar and alpine climates in the CORDEX FPS**

2 **LUCAS models: I. Evaluation of the snow-albedo effect**

3 Anne Sophie Daloz<sup>1</sup>, Clemens Schwingshackl<sup>1,13</sup>, Priscilla Mooney<sup>2</sup>, Susanna Strada<sup>3</sup>, Diana Rechid<sup>4</sup>,  
4 Edouard L. Davin<sup>5</sup>, Eleni Katragkou<sup>6</sup>, Nathalie de Noblet-Ducoudré<sup>7</sup>, Michal Belda<sup>8</sup>, Tomas Halenka<sup>8</sup>,  
5 Marcus Breil<sup>9</sup>, Rita M. Cardoso<sup>10</sup>, Peter Hoffmann<sup>4</sup>, Daniela C.A. Lima<sup>10</sup>, Ronny Meier<sup>5</sup>, Pedro M.M.  
6 Soares<sup>10</sup>, Giannis Sofiadis<sup>6</sup>, Gustav Strandberg<sup>11</sup>, Merja H. Toelle<sup>12</sup> and Marianne T. Lund<sup>1</sup>.

7 1. CICERO Center for International Climate Research, Oslo, Norway

8 2. NORCE Norwegian Research Centre, Bjerknes Centre for Climate Research, Bergen, Norway

9 3. International Center for Theoretical Physics, Trieste, Italy

10 4. Climate Service Center Germany, Helmholtz-Zentrum Hereon, Hamburg, Germany

11 5. Wyss Academy for Nature, Climate and Environmental Physics, Oeschger Center for Climate Change Research,  
12 University of Bern, Bern, Switzerland

13 6. Department of Meteorology and Climatology, School of Geology, Aristotle University of Thessaloniki,  
14 Thessaloniki, Greece

15 7. Laboratoire des Sciences du Climat et de l'environnement, Paris, France

16 8. Department of Atmospheric Physics, Faculty of Mathematics and Physics, Charles University, Prague, Czech  
17 Republic

18 9. Institute for Meteorology and Climate Research, Karlsruhe Institute of Technology, Karlsruhe, Germany

19 10. Instituto Dom Luiz, Faculdade de Ciências da Universidade de Lisboa, 1749-016 Lisboa, Portugal

20 11. Swedish Meteorological and Hydrological Institute, Norrköping, Sweden

21 12. Center for Environmental Systems Research, University of Kassel, Germany

22 13. Department of Geography, Ludwig-Maximilians-Universität, Munich, Germany.

23

24

25 *Corresponding author: Anne Sophie Daloz ([anne.sophie.daloz@cicero.oslo.no](mailto:anne.sophie.daloz@cicero.oslo.no))*

26

27



28 **Abstract**

29 In the Northern Hemisphere, the seasonal snow cover plays a major role in the climate system via its  
30 effect on surface albedo and fluxes. The parameterization of snow-atmosphere interactions in climate  
31 models remains a source of uncertainty and biases in the representation of the local and global climate.  
32 Here, we evaluate the ability of an ensemble of regional climate models (RCMs) coupled to different  
33 land surface models to simulate the snow albedo effect over Europe, in winter and spring. We use a  
34 previously defined index, the Snow Albedo Sensitivity Index (SASI), to quantify the radiative forcing  
35 due to the snow albedo effect. By comparing RCM-derived SASI values with SASI calculated from  
36 reanalyses and satellite retrievals, we show that an accurate simulation of snow cover is essential for  
37 correctly reproducing the observed forcing over mid- and high-latitudes in Europe. The choice of  
38 parameterizations with first and foremost the choice of the land surface model but also the convection  
39 scheme and the planetary boundary layer, strongly influences the representation of SASI as it affects the  
40 ability of climate models to simulate snow cover correctly. The agreement between the datasets differs  
41 between the accumulation and ablation periods, with the latter one presenting the greatest challenge for  
42 the RCMs. Given the dominant role of land surface processes in the simulation of snow cover during  
43 the ablation period, the results suggest that the choice of the land surface model is more critical for the  
44 representation of SASI than the atmospheric model during this time period.



45 **1. Introduction**

46 Snow is an important part of the climate system as it regulates the temperature of the Earth's  
47 surface via its effect on surface albedo and surface fluxes. In mid- and high-latitude regions, snow is the  
48 main interface through which land interacts with the atmosphere during the cold season and the  
49 importance of snow-atmosphere interactions in modulating the energy budget at high latitudes during  
50 winter has been demonstrated (Diro and Sushama, 2018; Henderson et al., 2018; Xu and Dirmeyer,  
51 2013). Snow cover extent and depth can modify both surface energy and moisture budgets, triggering  
52 complex feedback mechanisms that impact both local and remote climates (Diro and Sushama, 2018).  
53 In particular, snow can have a strong impact on climate due to its high albedo, primarily because of the  
54 contrast in the surface energy balance between snow-covered and snow-free land surfaces (Qu and Hall,  
55 2014). Reciprocally, with climate change, rising temperatures are already altering the Earth's snow  
56 amount and occurrences, for example shortening the snow season in Eurasia (Ye and Cohen, 2013;  
57 Gobiet et al., 2014; Mioduszewski et al., 2015; Beniston et al., 2018; Matiu et al., 2020). In this context,  
58 it is crucial to better understand snow-atmosphere processes and the ability of climate models to  
59 represent them.

60 The direct impact of snow on the atmosphere is known as the snow albedo effect (SAE; Xu and  
61 Dirmeyer, 2011, 2013), where the presence of snow affects the land surface energy budget and  
62 influences the local climate, modifying air temperature. To quantify the contribution from the SAE to  
63 the snow-atmosphere coupling, Xu and Dirmeyer (2011) developed the Snow Albedo Sensitivity Index  
64 (SASI). This index combines incoming shortwave radiation with snow cover variability to quantify the  
65 snow-albedo coupling strength, i.e. SASI estimates the degree to which the atmosphere responds to  
66 anomalies in snow cover. Applying SASI to satellite observations, Xu and Dirmeyer (2011) found that  
67 the coupling between snow and albedo is particularly strong during the snowmelt period in the Northern  
68 Hemisphere. At high-latitudes, for example, the effects of snow cover on the climate is strongly related  
69 to the way vegetation cover is prescribed. Removal of boreal forests locally reduces surface air  
70 temperature and precipitation by increasing surface albedo and decreasing plant evapotranspiration. The  
71 strength of the coupling between snow and the atmosphere is determined by processes involving



72 radiative fluxes but also hydrology. Therefore, Xu and Dirmeyer (2013) also defined the snow  
73 hydrological effect (SHE), which is a result of soil moisture anomalies from snowmelt. Through land-  
74 atmosphere interactions, they have a delayed impact on the atmosphere. Besides these direct and indirect  
75 effects, positive and negative snow-atmosphere feedbacks, such as the snow-albedo feedback (SAF; Qu  
76 and Hall, 2007; Fletcher et al., 2015; Thackeray et al., 2018) can amplify anomalies. The SAF represents  
77 changes in surface albedo from cooling (warming) that can cause decreases (increases) in absorbed solar  
78 radiation, amplifying the initial cooling (warming). It is an important driver for regional climate change  
79 in Northern Hemisphere land areas.

80 Here, we investigate the ability of an ensemble of RCMs to represent snow cover and the  
81 radiative forcing from the snow albedo effect (SASI) over Europe, including a comparison between mid-  
82 and high-latitude regions. We derive SASI using radiative fluxes and snow cover from satellites,  
83 reanalysis and model outputs. Building on findings by Xu and Dirmeyer (2011, 2013), we focus on  
84 winter and spring seasons, i.e. transitioning from the accumulation to the ablation period, when SASI is  
85 reaching a maximum. While some previous studies have investigated snow-atmosphere processes in  
86 climate models for specific regions (e.g. European Alps; Magnusson et al., 2010; Matiu et al., 2019;  
87 Lüthi et al., 2019), the literature remains limited. Here, we use the RCMs outputs from the flagship pilot  
88 study Land Use and Climate Across Scale (LUCAS; Rechid et al., 2017; Breil et al., 2020; Davin et al.,  
89 2020; Reinhart et al., 2020; Sofiadis et al., 2021). It is endorsed by the Coordinated Regional Climate  
90 Downscaling Experiment (CORDEX) of the World Climate Research Programme (WCRP) over the  
91 European domain (EURO-CORDEX, Jacob et al., 2020) and it enables us to perform a broader  
92 assessment of several RCMs within a consistent framework. Our assessment is carried out in two parts  
93 and published in companion articles. In Part I, we investigate the ability of these RCMs to represent the  
94 SASI under present-day land cover distribution, while in Part II we explore the effects of large-scale  
95 changes in vegetation cover. In LUCAS, each RCM performed three coupled land-atmosphere  
96 experiments at the European scale: two idealized and intensive land use change experiments (GRASS  
97 and FOREST) and a control experiment (EVAL). The GRASS and FOREST experiments will be



98 examined in the companion paper (Part II) while here, we use ten models from the EVAL experiment  
99 only, which employ their standard land use and land cover maps.

100 Section 2 introduces the modeling and observational datasets used in this study as well as the  
101 derivation of SASI, while Section 3 examines and discusses the ability of climate models to represent  
102 SASI compared with satellite observations and reanalyses, focusing on the strength and timing of the  
103 signal. Further, the origin of the differences between the models are explored by evaluating potential  
104 common biases in the ensemble of simulations as well as individual model biases. The analysis also  
105 explores the differences in SASI between mid- and high-latitude regions, opening the discussion on the  
106 impacts of different land cover for the simulation of SASI, which will be further explored in Part II.  
107 Finally, Section 4 the last sections offer some concluding remarks.

## 108 **2. Data and methodology**

### 109 **2.1 LUCAS experiments and models**

#### 110 **2.1.1 The LUCAS experiments**

111 The simulations from the flagship pilot study LUCAS simulations cover the standard EURO-  
112 CORDEX domain (Jacob et al., 2014) with a horizontal grid resolution of  $0.44^\circ$  (around 50 km). All  
113 RCMs in LUCAS use a rotated coordinate system except the RegCM model, which applies a Lambert  
114 conformal projection (suitable for mid-latitudes) on a regular grid. Here we use outputs from the EVAL  
115 experiment, which employ land use and land cover maps; the GRASS and FOREST experiments will  
116 be examined in the companion paper (part II). All simulations span the period 1986–2015 (with a spin-  
117 up period ranging from one up to six years depending on the model) and take lateral and boundary  
118 conditions from the ERA-Interim reanalysis (Dee et al., 2011). More details can be found in Davin et  
119 al. (2020).

#### 120 **2.1.2 Models and configurations**

121 We use outputs from ten coupled surface-atmosphere RCM simulations that participated in the  
122 LUCAS project. The main model characteristics that are important for snow albedo coupling are  
123 summarized in Table 1. The model ensemble presents five different RCMs: COSMO-CLM version 5.0-  
124 clm9 (Sørland et al., 2021), WRF version 3.8.1 (Skamarock et al., 2008), RegCM versions 4.6 and 4.7



125 (Giorgi et al., 2012), RCA4 (Strandberg et al., 2015) and REMO (Jacob et al., 2012). These RCMs  
126 contributed with different setups and configurations as described in Table 1. For example, the same  
127 RCM is coupled to different land surface models (LSMs): COSMO-CLM is coupled to three distinct  
128 LSMs, which are CLM5.0 (Lawrence et al., 2020), VEG3D (Breil and Schadler, 2017) and TERRA-  
129 ML (Schrodin and Heise, 2002). WRF is coupled with either CLM4.0 (Oleson et al., 2010) or NOAH-  
130 MP (Niu et al., 2011). Vice versa, the same LSM is combined with different versions of RCMs. The  
131 CLM4.5 (Oleson et al., 2013) LSM is coupled to two distinct versions of RegCM (4.6 and 4.7) which  
132 also differ in their choice of convection schemes. There are also two institutes with the same RCM and  
133 LSM (WRF and Noah-MP) but different parameterizations, as they use distinct planetary boundary layer  
134 (PBL) schemes. A detailed description of the RCMs is provided by Davin et al. (2020). For the analyses  
135 in the present study, we use daily and monthly model outputs for incoming shortwave radiation and  
136 snow cover. For deriving SASI, the native grid of the models was kept, minimising data loss. The other  
137 fields were interpolated to a common  $0.5^\circ \times 0.5^\circ$  grid using Climate Data Operators (CDO) bilinear  
138 remapping.

### 139 **2.1.3 Snow-buried fraction of vegetation in models**

140 At high-latitudes, the effects of snow cover on regional climate strongly depend on the  
141 prescribed vegetation cover. Removal of boreal forests locally reduces surface air temperature and  
142 precipitation by increasing surface albedo and the duration of the snow cover and by decreasing plant  
143 evapotranspiration. Today, the role of forest albedo on winter-spring climate in the high-latitudes is well  
144 acknowledged based on field campaigns such as the Boreal Ecosystem-Atmosphere Study (BOREAS;  
145 Betts et al., 2001) and on modeling studies (e.g., Betts and Ball, 1997; Betts et al., 1996; Betts et al.,  
146 2001; Bonan, 2008; Davin and Noblet-Ducoudré, 2010; Mooney et al., 2021). These studies led to  
147 implementing more sophisticated snow sub-models in LSMs that account for the burial of vegetation by  
148 snow cover.

149 In the LUCAS ensemble, all LSMs, except for the TERRA-ML LSM used by CCLM-TERRA,  
150 adjust the effective Leaf and Stem Area Index for snow-buried vegetation by adopting similar  
151 approaches. Being a bulk/one-dimensional LSM, TERRA-ML applies an infinitesimal vegetation layer



152 on top of the soil surface and has no canopy (i.e., vegetation lays flat on the surface). However, to  
153 correctly simulate the effect of trees masking the ground snow on radiation, TERRA-ML applies a  
154 reduction factor for the snow albedo when vegetation such as forest canopies masks the snow. Hence,  
155 when vegetation is snow-buried, all LSMs account for a highly reflecting surface in the calculation of  
156 surface albedo. In Table 1, interested readers may find references to RCM-dependent snow-buried  
157 vegetation schemes.

158 In terms of snow schemes, some LSMs contain more sophistication than others. Compared to  
159 previous CLM versions (i.e., CLM4.0 and CLM4.5), CLM5.0 used by CCLM-CLM5.0 counts more  
160 snow layers (12 instead of 5), treats separately canopy intercepted snow and more realistically captures  
161 temperature and wind effects on the density of fresh snow (Lawrence et al., 2020; van Kampenhout et  
162 al., 2017). The RCA4 model system and its internal LSM, used in RCA, include sub-grid orography in  
163 the snow cover to capture inhomogeneous snow cover in mountainous areas. Noah-MP allows for 3  
164 snow layers, depending on the total snow depth. To provide a better representation of the ground heat  
165 fluxes, the first very layer is only 0.045 m thick. Noah-MP also considers snow interception by the  
166 canopy, accounting for wind and temperature effects on snow accumulation and precipitation from the  
167 canopy, snow melting and refreezing (Niu and Yang, 2004). The ground snow cover fraction is a  
168 function of the snow depth and density and ground roughness (Niu et al., 2007)

## 169 **2.2 Reanalyses and remote sensing data**

170 Reanalysis data from ERA5-Land (Muñoz Sabater, 2019; Muñoz Sabater et al., 2021) and  
171 MERRA-2 (Gelaro et al., 2017) as well as satellite data from the Moderate Resolution Imaging  
172 Spectroradiometer (MODIS; Hall and Riggs, 2016) are used to evaluate the modelled snow distribution  
173 and radiation in the RCMs. Specifically, we use monthly data for snow cover (variable “fractional area  
174 of land snow cover” in MERRA-2), incoming shortwave radiation from ERA5-Land and MERRA-2,  
175 and daily snow cover data from the MODIS sensors AQUA and TERRA. The reanalysis data are  
176 interpolated bilinearly to the common  $0.5^\circ \times 0.5^\circ$  grid (see Section 2.2). Reanalysis data cover the time  
177 period 1986-2015 and MODIS data the period 2003-2015.

178 For MODIS data, the following processing steps are applied:



- 179 1. Data are masked according to the prevailing cloud cover since high cloud cover prevents a  
180 correct estimation of snow cover. We apply two different thresholds (20% and 50%) to the  
181 percent of clouds in each cell.
- 182 2. Only data flagged as “best”, “good”, and “ok” are used while all other data are masked.
- 183 3. Data are conservatively remapped to the common 0.5°x0.5° grid. Conservative remapping is  
184 chosen due to the large difference in resolution between the original MODIS data (0.05°) and  
185 the target grid (0.5°). It considers all grid points in the interpolation while, e.g., bilinear  
186 interpolation would only consider the neighbouring grid cells of the target grid.
- 187 4. A land-sea mask is applied to make sure that only land grid points are included in the analysis.  
188 Only grid points with more than 50% land fraction are included.

189 The masking for MODIS data implies that single grid points can contribute differently to the average  
190 over one region. To make the models and reanalyses comparable, each grid point is weighted by the  
191 amount of available MODIS data (individually for each month of the whole time period).

192

### 193 **2.3 Snow Albedo Sensitivity Index (SASI) and geographical scope**

194 SASI is an index that quantifies the climate forcing due to the snow albedo effect (Xu and  
195 Dirmeyer, 2013). It is defined as:

$$196 \quad SASI = SW * \sigma(f_{sno})\Delta\alpha \quad (1)$$

197 where  $SW$  is the net shortwave radiation at the surface,  $\sigma(f_{sno})$  is the standard deviation of snow cover  
198 fraction, and  $\Delta\alpha$  is the average difference between the albedo of a snow-covered surface and the albedo  
199 of a snow-free surface.  $\Delta\alpha$  is a constant value of 0.4 as assumed in Xu and Dirmeyer (2013). SASI is in  
200  $Wm^{-2}$  and high values of SASI, such as  $10 Wm^{-2}$ , indicate a strong climate forcing from the snow albedo  
201 effect (Xu and Dirmeyer, 2013).

202 To better understand geographical differences in the role of snow for land-atmosphere coupling,  
203 we focus on three sub-regions over Europe, with different climate, vegetation cover, topography or  
204 latitudes: Scandinavia [5°E-30°E, 55°N-70°N], East Europe [16 °E-30°E, 44°N-55°N] and East Baltic  
205 [20°E-40°E, 50°N-62°N] (see Figure 1). The first two regions, Scandinavia and East Europe correspond





206 to regions 8 and 5 of the PRUDENCE project (Prediction of Regional scenarios and Uncertainties for  
207 Defining European Climate change risk and Effects; Christensen and Christensen, 2007). The three  
208 selected regions differ in terms of climate but also in terms of vegetation: vegetation in Scandinavia is  
209 mostly trees while the two other regions are covered by cropland and trees. The Scandinavian region  
210 also stands out because of its geographical location covering high latitudes, where the incoming  
211 shortwave radiation is very small or zero during winter. In comparison with the East Baltic region, which  
212 is covered by plains, the East Europe and Scandinavia regions have a more complex topography as they  
213 encompass the Carpathian and Scandinavian mountains, respectively.

214

### 215 **3. Results and discussion**

#### 216 **3.1 SASI in satellite observations, reanalyses and RCMs over Europe**

217 In Figure 2, we first show the geographical distribution of SASI over Europe based on satellite  
218 observations, the ERA5-Land reanalysis and the LUCAS models from January to June, averaged over  
219 the 1986-2015 period. Focusing first on the satellite observations and ERA5-Land, an increase in SASI  
220 can be observed during the first months of the year when solar radiation increases and snow is  
221 accumulating (accumulation period), reaching a maximum in March or April depending on the region  
222 examined, and then decreasing when snow starts melting (ablation period). At higher latitudes snow  
223 melts later than at mid-latitudes, giving rise to SASI values during spring, as shown in Figure 2. Then,  
224 SASI reaches very low values in May and June when the snow has melted almost entirely. This is as  
225 expected, and the overall seasonal trend is consistent with Xu and Dirmeyer (2013). The model data  
226 exhibits the same overall spatiotemporal cycle in SASI as the satellite observations and ERA5-Land.  
227 However, large differences can be seen between the simulations in terms of amplitude or pattern,  
228 especially during the ablation period. In March over the Carpathian Mountains, for example, SASI varies  
229 between  $1 \text{ Wm}^{-2}$  for WRFa-NoahMP and RCA, and  $10 \text{ Wm}^{-2}$  for CCLM-CLM5.0 and RegCMa-  
230 CLM4.5. It is also noteworthy that for almost all the models, SASI is close to zero everywhere in  
231 continental Europe in May and June, as the snow has almost entirely melted, while in May for RegCMb-  
232 CLM4.5 and CCLM-VEG3D there are still high values of SASI ( $\sim 10 \text{ Wm}^{-2}$ ).

233



234           The ensemble of simulations run for LUCAS enable us to discuss the role of different  
235 components of the RCMs, such as the land and atmosphere models or the choice in parameterizations.  
236 For example, WRFc-NoahMP and WRFa-NoahMP show noticeable differences in the amplitude and  
237 pattern of SASI (Fig. 2), even though they use the same LSM (Noah-MP) and atmospheric model  
238 (WRF). Their differences come from parameterizations (planetary boundary layer and convection), thus  
239 demonstrating the importance of atmospheric processes and their model representation for representing  
240 snow processes. Then, WRF configuration coupled with the LSM CLM4.0 (WRFb-CLM4.0) also shows  
241 different results from when it is coupled with NOAH-MP. For example, WRFa-NoahMP shows an  
242 earlier poleward migration of high SASI values compared to WRFb-CLM4.0, moving north about one  
243 month before WRFb-CLM4.0. Large differences can also be observed between CCLM-CLM5.0,  
244 CCLM-TERRA, and CCLM-VEG3D; they all use the same RCM but different LSMs. In contrast to the  
245 two other Cosmo configurations, CCLM-VEG3D uses a snow flag for snow cover (i.e., indicates if snow  
246 is present or not; Section 2.3), explaining its different representation of SASI. This suggests that SASI  
247 is very sensitive to the configurations of and process parameterizations in the climate model. In  
248 particular, the choice of the LSM or certain parameterizations (e.g. convection scheme) highly influence  
249 the representation of the climate forcing from the snow albedo effect. The role of the LSM in this context  
250 will be investigated further in the coming sections of the article.

251

### 252 **3.2 Transition between the accumulation and ablation periods**

253

254           To further investigate the differences in snow albedo coupling between the simulations and the  
255 observation-based datasets during the accumulation and ablation periods, a time-series of SASI from  
256 January to June is presented in Figure 3 for the three sub-regions East Europe, East Baltic and  
257 Scandinavia (see Figure 1 for their extents). Before looking at the differences between the different  
258 datasets, it is interesting to compare the amplitude of SASI between East Baltic and East Europe (mid-  
259 latitude regions) with Scandinavia (high-latitude region), which shows slightly higher values of SASI  
260 over the mid-latitude regions in satellite observations, ERA5 and most of the RCMs. This confirms  
261 previous findings from Xu and Dirmeyer (2013), which estimated higher values of SASI in mid- versus



262 high-latitude regions in satellite observations. However, even with higher values at mid-latitudes, this  
263 result suggests that the radiative forcing due to the snow albedo effect is not negligible over high-latitude  
264 regions in winter and spring. This result shows again the importance of the snow-atmosphere processes  
265 in mid- and high-latitudes in the Northern hemisphere.

266 Then, coming back to the comparison of the different datasets, in all three regions, the models  
267 and observations indicate a pronounced peak in SASI. The maximum in SASI marks the transition  
268 between the accumulation and ablation periods. The timing of this transition depends on the region  
269 examined due to, for example, latitudinal differences in incoming solar radiation. Although the  
270 amplitude of the peak is very similar between the satellite observations and ERA5-Land, it is interesting  
271 to see that the timing differs between them, over Scandinavia and East Baltic. Over East Europe it  
272 happens in March for both the satellite observations and ERA5, for East Baltic in March (satellites) or  
273 April (ERA5) and for Scandinavia in April (satellites) or May (ERA5). The origin of these differences  
274 has not been clarified yet. This might be due to the higher elevations of these two regions compared to  
275 East Europe as complex orography is a driving factor for the spatial heterogeneity of precipitation  
276 (Grunewald et al., 2014).

277 The LUCAS simulations also show a pronounced peak in SASI in all regions (Fig. 3), however  
278 they do not all agree on the timing and the amplitude of the signal. For example, in the East Baltic  
279 region, some models (WRFc-NoahMP and WRFa-NoahMP) simulate a peak in March, others in April  
280 (WRFb-CLM4.0 and CCLM-CLM5.0) or even in May (RegCMb-CLM4.5 and CCLM-VEG3D). In  
281 general, RegCMb-CLM4.5 and CCLM-VEG3D tend to present the latest peak in SASI as well as the  
282 highest amplitude in the signal. On the other hand, WRFa-NoahMP tends to produce an earlier peak and  
283 lower values of SASI, especially over East Europe. These differences might be related to the way snow  
284 melts in the different models and will be further explored in the next section. More generally, we see  
285 that during the accumulation period, all the datasets are in better agreement compared to the ablation  
286 period (Fig. 3). For East Europe and East Baltic, the spread largely increases in March and for  
287 Scandinavia from April until the end of the season, when the snow is melting.

288 This large model spread during the ablation period is further confirmed by Figure 4 showing the  
289 pattern correlation between the simulations and ERA5-Land from January to June. For many models,



290 the correlation is high at the beginning of the season but strongly decreases in March or April, when the  
291 snow starts melting. These results are in agreement with previous studies showing the difficulties of  
292 climate models to represent snow processes during the ablation period (Essery et al. 2009). Given the  
293 dominant role of land surface processes during the ablation period, this suggests that the choice of the  
294 LSM is more critical for the representation of the climate forcing from the snow albedo effect than the  
295 atmospheric model in spring. For calculating snow-covered areas at different stages of ablation, a correct  
296 representation of the landscape type is important (Pomeroy et al., 1998). Figure 4 also shows that the  
297 behavior of the RCMs is different between East Europe and East Baltic versus Scandinavia. Over the  
298 latter region, most RCMs differ from the reanalysis indicated by low correlations. Earlier studies showed  
299 that snow accumulates or melts very differently in an open region compared to a forested region (Jonas  
300 and Essery, 2014; Moeser et al., 2016). Our results suggest that RCMs represent snow processes better  
301 in open spaces like the East Baltic than in forest-covered regions like Scandinavia. The relationship  
302 between the representation of SASI and land cover will be further explored in the companion article,  
303 Part II. The mountains in Scandinavia could also be a source of biases since the resolution of the RCM  
304 simulations ( $0.44^\circ$ ) can be considered insufficient to represent the more complex topography of  
305 Scandinavia.

306

### 307 **3.3 Inter-model differences in SASI**

308 To better understand the origin of the differences in SASI across RCMs, we explore the  
309 relationship between SASI and its components, surface snow cover and shortwave radiation, during the  
310 accumulation and ablation periods. Figure 5 presents a comparison of the averaged monthly surface  
311 snow cover for the LUCAS simulations, the reanalyses MERRA-2 and ERA5-Land as well as the  
312 satellite observations from MODIS, averaged over our three regions of interest, from January to May.  
313 First, it should be noted that differences can be observed between the reanalyses and the satellite  
314 observations as the different datasets have their own limitations or biases. For example, the surface snow  
315 cover in East Baltic in March is  $\sim 0.6$  for MODIS,  $\sim 0.7$  for MERRA-2 and  $\sim 0.8$  for ERA5-Land. It is  
316 therefore important to include several observation-based datasets to evaluate the ability of climate  
317 models to represent snow cover and estimate the uncertainties associated with this variable. The



318 representation of snow cover in RCMs can also be different depending on the model examined. Over  
319 Scandinavia, snow cover varies between 0.4 for WRFa-NoahMP and 1.0 for WRFb-CLM4.0 in January.  
320 For the same month, the differences are even higher for the other two regions, varying between 0.3 for  
321 WRFa-NoahMP and 1.0 for WRFb-CLM4.0 in East Baltic, and 0.1 for WRFa-NoahMP and 1.0 for  
322 WRFb-CLM4.0 in East Europe. Although there are already differences during the accumulation period,  
323 Figure 5 shows that the spread increases when the snow starts melting. This result indicates a common  
324 bias between the models that highly disagree with the reanalysis and observations, regarding snow cover  
325 in spring. This confirms the result from the previous section as it is again pointing towards a bias from  
326 LSMs as this part of the RCM is primordial for representing land surface processes related to snow cover  
327 during the ablation period.

328         Based on Figure 3, RegCmb-CLM4.5 and CCLM-VEG3D were identified as models with  
329 higher values in SASI during the ablation period and later peaks for all regions. Figure 5 shows that this  
330 behavior can be at least partly attributed to their representation of snow cover. During the ablation  
331 period, they all tend to produce higher values of snow cover compared to the other models and also to  
332 keep high values later in the season. This behavior is confirmed by the black dots under these two models  
333 during the ablation period as they indicate when the models are outside the range of the reference  
334 datasets (MERRA-2, ERA5-Land and MODIS). This is particularly striking for CCLM-VEG3D.  
335 Similarly, the low SASI peaks for WRFa-NoahMP, which also occur earlier than the peaks for other  
336 models (Figure 3), might be related to the lower values in snow cover and the small interannual snow  
337 cover variability compared to the other RCMs, particularly in East Europe (Figure 5). Again, this is  
338 confirmed by the black dots indicated under the model. The differences in snow cover are also reflected  
339 by the rate of snow melting for the different RCMs (Supplemental Material; Figure S1). The models  
340 having high snow cover late in spring (RegCmb-CLM4.5 and CCLM-VEG3D) tend to have later snow  
341 melt than the other models while WRFa-NoahMP, showing reduced snow cover earlier than the other  
342 models, tends to melt sooner.

343         Another component of SASI is shortwave radiation at the surface, which is presented in Figure  
344 6 for the LUCAS simulations, the reanalyses MERRA-2 and ERA5-Land, averaged over our three  
345 regions of interest, from January to May. The comparison between the RCMs and the reanalysis shows



346 noticeable differences for some models. Both REMO-iMOVE and CCLM-VEG3D exhibit very  
347 different results in terms of surface shortwave radiation compared to the datasets as shown by the black  
348 dots on the figure, showing much lower and higher values, respectively. However, even with these  
349 discrepancies, they both reproduce SASI reasonably well. This seems to indicate that the differences in  
350 the representation of the forcing from the snow albedo effect are mostly driven by differences in the  
351 representation of snow cover in the models. This is confirmed by Figure 7 showing the average  
352 correlation across models between SASI and shortwave radiation (left) as well as SASI and snow cover  
353 (right) for the LUCAS models. Scandinavia and East Baltic present similar results with significant,  
354 positive correlations between SASI and snow cover for almost all months, associated with positive but  
355 not significant correlations between SASI and shortwave radiation. For East Europe, the correlation  
356 between SASI and snow cover is low and not significant in January and February but remains high and  
357 significant the rest of the time period. In parallel, the correlation between SASI and downward  
358 shortwave radiation at the surface is negative for almost all months and not significant. Overall, high  
359 and significant correlations often appear between SASI and snow cover for the three regions from  
360 January to June. On the other hand, the correlations between SASI and shortwave radiation are low and  
361 usually not significant. This indicates that the differences in the representation of the forcing from the  
362 snow albedo effect are mostly driven by differences in the representation of snow cover in the models.

363

#### 364 **4. Conclusion**

365 Previous work already showed the difficulty for climate models to represent snow variables or  
366 processes, such as snow cover and depth (Matiu et al., 2020) or the SAF (Fletcher et al., 2015), however  
367 the origin of the differences between the models is not clear yet. In this work, we focus on the ability of  
368 RCMs to simulate the radiative forcing from the snow albedo effect in winter and spring over Europe  
369 and explore the origin of the differences between the RCMs. This forcing is represented by the index  
370 SASI, which quantifies the strength of the coupling between snow and albedo. Ten RCMs from the  
371 CORDEX Flagship Pilot Study LUCAS are compared to satellite observations and reanalysis including  
372 ERA5-Land and MERRA-2. These simulations are part of the control experiment of LUCAS, which



373 uses the standard EURO-CORDEX domain (Jacob et al., 2014) with a horizontal grid resolution of 0.44°  
374 (around 50 km).

375 The results show that climate models are able to reproduce some of the SASI characteristics  
376 (e.g. existence of a peak, amplitude of the peak) compared to reanalysis and satellite observations  
377 (Section 3.1), even if large differences appear between the RCMs. The climate models' ability to  
378 represent SASI is highly related to their representation of snow cover (Section 3.3), which can be  
379 difficult to represent for climate models (Matiu et al., 2020). Our results also suggest that the models'  
380 capability highly differs between the accumulation and ablation periods. Most models have much lower  
381 agreement with reanalyses and satellite observations in the ablation period, with some exceptions (e.g.  
382 CCLM-CLM5.0 over East Europe), indicating a common bias regarding snow cover in spring, pointing  
383 towards a bias from LSMs. This bias seems to be common to most LSMs even if they are based on  
384 different assumptions and parameterizations (see Section 2.3). It is also interesting that even though  
385 CCLM-TERRA is not as advanced in terms of snow modeling compared to the other models (e.g.  
386 Section 2.1.3), it still manages to represent SASI reasonably well over Europe. In addition, the  
387 representation of the sub-grid scale surface heterogeneity (Table 1; PFT-dominant versus PFT-tile) does  
388 not seem to affect the ability of RCMs to represent snow cover or SASI.

389 Although it is difficult to identify the origin of the bias in the RCMs, an increase in spatial  
390 resolution might improve the simulation of snow cover and therefore the representation of SASI. For  
391 example, over Scandinavia, an increase in spatial resolution would provide a better representation of the  
392 complex topography of the region as well as its forested areas, which may lead to an improved  
393 simulation of the coupling between snow and albedo. The coming phases of LUCAS, phases 2 and 3,  
394 could help answer this question as they will produce simulations at a higher spatial resolution, 12 km  
395 and convection-permitting (<3km) respectively. Taking advantage of the different configurations of the  
396 LUCAS simulations, we have also explored the role of distinct parts of the models in their ability to  
397 represent SASI. The first part of this work has already emphasized the role of the LSMs, but other  
398 components can also play an important role. WRFc-NoahMP and WRFa-NoahMP, even though using  
399 the same RCM and LSM, show noticeable differences in the amplitude and pattern of SASI. Their



400 differences in parameterizations (planetary boundary layer and convection) are certainly affecting the  
401 way they represent SASI, highlighting the impact of such choices and the role of atmospheric processes.

402 Mid- and high-latitude areas are also specifically examined looking at three sub-regions:  
403 Scandinavia, East Europe and East Baltic (Section 3.2). The comparison of the three sub-regions shows  
404 the difficulties for models to simulate SASI over Scandinavia during the accumulation and ablation  
405 periods. The simulation of snow processes in a forested region is more challenging than in an open  
406 region (Jonas and Essery, 2014; Moeser et al., 2016). Thus, potentially climate models can have more  
407 difficulties representing snow processes in forest-covered regions like Scandinavia compared to open-  
408 land regions like East Baltic. The relationship between the representation of SASI and land-cover will  
409 be further explored in the companion article (Part II), analyzing the other experiments (GRASS and  
410 FOREST) from LUCAS. Finally, the comparison of mid- versus high-latitude regions shows slightly  
411 higher values of SASI over the mid-latitude regions in satellite observations, ERA5 and most of the  
412 RCMs. This confirms previous findings from Xu and Dirmeyer (2013), which estimated higher values  
413 of SASI in mid- versus high-latitude regions in satellite observations. Our results also suggest that the  
414 climate forcing due to the snow albedo effect is not negligible over high-latitude regions in winter and  
415 spring. This is important since often the land-atmosphere coupling is considered weaker at higher  
416 latitudes (Xu and Dirmeyer, 2011) but it is also possible that this coupling happens through snow and is  
417 therefore underestimated.

418

#### 419 **Acknowledgements**

420 CICERO researchers acknowledge funding from the Norwegian Research Council (grant 254966). In  
421 Norway, the simulations were stored on the server NIRD with resources provided by UNINETT Sigma2  
422 - the National Infrastructure for High Performance Computing and Data Storage in Norway. WRFc-  
423 NoahMP simulations were performed and stored on resources provided by UNINETT Sigma2 - the  
424 National Infrastructure for High Performance Computing and Data Storage in Norway (NN9280K,  
425 NS9001K, NS9599K). WRFb-CLM4.0 simulations were supported by computational time granted from  
426 the National Infrastructures for Research and Technology S.A. (GRNET S.A.) in the National HPC





427 facility - ARIS - under project ID pr005025 and pr007033\_thin. Edouard L. Davin and Ronny Meier  
428 acknowledge financial support from the Swiss National Science Foundation (SNSF) through the  
429 CLIMPULSE project and thank the Swiss National Supercomputing Centre (CSCS) for providing  
430 computing resources. P. Hoffmann is funded by the Climate Service Center Germany (GERICS) of the  
431 Helmholtz-Zentrum Hereon in the frame of the Helmholtz-Institut Climate Service Science (HICSS)  
432 project LANDMATE. The authors gratefully acknowledge the WCRP CORDEX Flagship Pilot Study  
433 LUCAS "Land use and Climate Across Scales" and the research data exchange infrastructure and  
434 services provided by the Jülich Supercomputing Centre, Germany, as part of the Helmholtz Data  
435 Federation initiative. R. M. Cardoso, D. C. A. Lima P. M. M. Soares were supported by national funds  
436 through FCT (Fundação para a Ciência e a Tecnologia, Portugal) under project LEADING (PTDC/CTA-  
437 MET/28914/2017), and project UIDB/50019/2020. This study contains modified Copernicus Climate  
438 Change Service Information 2021. ERA5-Land data are available at  
439 <https://doi.org/10.24381/cds.e2161bac> and <https://doi.org/10.24381/cds.68d2bb30>. The information  
440 related to GlobSnow data is presented in <https://doi.org/10.1016/j.rse.2014.09.018>. Variables from  
441 MERRA2 have been downloaded in 2019 and 2020 via NASA/GSFC, Greenbelt, MD, USA, NASA  
442 Goddard Earth Sciences Data and Information Services Center (GES DISC).

443

#### 444 **References:**

445 Beniston, M., Farinotti, D., Stoffel, M., Andreassen, L.M., Coppola, E., Eckert, N., Fantini, A.,  
446 Giacona, F., Hauck, C., Huss, M., Huwald, H., Lehning, M., López-Moreno, J.I., Magnusson, J., Marty,  
447 C., Morán-Tejeda, E., Morin, S., Naaim, M., Provenzale, A., Rabatel, A., Six, D., Stötter, J., Strasser,  
448 U., Terzago, S., Vincent, C., The European mountain cryosphere: A review of its current state, trends,  
449 and future challenges, *Cryosphere*, 12 (2), pp. 759-794, 2018.

450 Betts, A. K., Ball, J. H., Beljaars A. C. M., Miller, M. J. and Viterbo, P. A.: The land surface-  
451 atmosphere interaction: A review based on observational and global modeling perspectives, *Journal of*  
452 *Geophysical Research: Atmospheres*. 101(D3), 7209-7225, 10.1029/95jd02135, 1996.



- 453 Betts, A. K. & Ball, J. H.: Albedo over the boreal forest, *Journal of Geophysical Research:*  
454 *Atmospheres*. 102(D24), 28901-28909, 10.1029/96jd03876, 1997.
- 455 Betts, A. K., Ball, J. H. and McCaughey, J. H.: Near-surface climate in the boreal forest, *Journal*  
456 *of Geophysical Research: Atmospheres*. 106(D24), 33529-33541, 10.1029/2001jd900047, 2001.
- 457 Bonan, G. B.: Forests and Climate Change: Forcings, Feedbacks, and the Climate Benefits of  
458 Forests, *Science*. 320(5882), 1444-1449, 10.1126/science.1155121, 2008.
- 459 Braun, F. J., & Schädler G.: Comparison of soil hydraulic parameterizations for mesoscale  
460 meteorological models. *Journal of Applied Meteorology*, 44(7), 1116-1132, 2005.
- 461 Breil, M., & Schädler, G.: Quantification of the uncertainties in soil and vegetation  
462 parameterizations for regional climate simulations in Europe. *Journal of Hydrometeorology*, 18(5),  
463 1535-1548, 2017.
- 464 Breil, M., Rechid, D., Davin, E., de Noblet-Ducoudré, N., Katragou, E., Cardoso, R., Hoffmann  
465 P., Jach, L., Soares, P., Sofiadis, G., Strada, S., Strandberg, G., Toelle, M., Warrach-Sag, K.: The  
466 opposing effects of afforestation on the diurnal temperature cycle at the surface and in the atmospheric  
467 surface layer in the European summer. *Journal of Climate*, 33 (21), pp. 9159-9179, 2020.
- 468 C3S: Copernicus Climate Change Service (C3S) (2017): ERA5: Fifth generation of ECMWF  
469 atmospheric reanalyses of the global climate . Copernicus Climate Change Service Climate Data Store  
470 (CDS), date of access 200414. <https://cds.climate.copernicus.eu/cdsapp#!/home>, 2017.
- 471 Christensen, J.H., and Christensen, O.B.: A summary of the PRUDENCE model projections of  
472 changes in European climate by the end of this century. *Climatic Change* 81, 7–30.,  
473 <https://doi.org/10.1007/s10584-006-9210-7>, 2007.
- 474 Davin, E. L., & Noblet-Ducoudré, N. D.: Climatic Impact of Global-Scale Deforestation:  
475 Radiative versus Nonradiative Processes, *Journal of Climate*. 23(1), 97-112, 10.1175/2009jcli3102.1,  
476 2010.
- 477 Davin, E. L., Rechid, D., Breil, M., Cardoso, R. M., Coppola, E., Hoffmann, P., Jach, L. L.,  
478 Katragkou, E., de Noblet-Ducoudré, N., Radtke, K., Raffa, M., Soares, P. M. M., Sofiadis, G., Strada,  
479 S., Strandberg, G., Tölle, M. H., Warrach-Sagi, K. & Wulfmeyer, V.: Biogeophysical impacts of



480 forestation in Europe: first results from the LUCAS (Land Use and Climate Across Scales) regional  
481 climate model intercomparison, *Earth Syst. Dynam.* 11(1), 183-200, 10.5194/esd-11-183-2020, 2020.

482 Deardorff, J.: Efficient prediction of ground surface temperature and moisture, with inclusion of  
483 a layer of vegetation, *J. Geophys. Res.*, 83(4), 1889–1903, doi:[10.1029/JC083iC04p01889](https://doi.org/10.1029/JC083iC04p01889), 1978.

484 Dee, D. P., Uppala, S. M., Simmons, A. J., Berrisford, P., Poli, P., Kobayashi, S., Andrae, U.,  
485 Balmaseda, M. A., Balsamo, G., Bauer, P., Bechtold, P., Beljaars, A. C. M., van de Berg, L., Bidlot, J.,  
486 Bormann, N., Delsol, C., Dragani, R., Fuentes, M., Geer, A. J., Haimberger, L., Healy, S. B., Hersbach,  
487 H., Hólm, E. V., Isaksen, L., Kållberg, P., Köhler, M., Matricardi, M., McNally, A. P., Monge-Sanz, B.  
488 M., Morcrette, J.-J., Park, B.-K., Peubey, C., de Rosnay, P., Tavolato, C., Thépaut, J.-N., & Vitart, F.:  
489 The ERA-Interim reanalysis: configuration and performance of the data assimilation system, *Quarterly*  
490 *Journal of the Royal Meteorological Society.* 137(656), 553-597, 10.1002/qj.828, 2011.

491 Diro, G. T., & Sushama, L.: Snow–precipitation coupling and related atmospheric feedbacks  
492 over North America, *Atmospheric Science Letters.* 19(8), e831, 10.1002/asl.831, 2018.

493 Doms, G., Förstner, J., Heise, E., Herzog, H.-J., Mironov, D., Raschendorfer, M., Reinhardt, T.,  
494 Ritter, Schrodin, B.R., Schulz, J.-P., Vogel G.: A Description of the Nonhydrostatic Regional Model  
495 LM, Part II: Physical Parameterization. DWD, 2013.

496 Essery, R., and Coauthors, 2009: SNOWMIP2: An Evaluation of Forest Snow Process  
497 Simulations. *Bull. Amer. Meteor. Soc.*, **90**, 1120–1136, <https://doi.org/10.1175/2009BAMS2629.1>.

498 Fletcher, C. G., Thackeray, C. W., and Burgers, T. M.: Evaluating biases in simulated snow  
499 albedo feedback in two generations of climate models, *J. Geophys. Res. Atmos.*, 120, 12– 26,  
500 doi:[10.1002/2014JD022546](https://doi.org/10.1002/2014JD022546), 2015.

501 Gelaro R., McCarty W., Suárez M. J., Todling R., Molod A., Takacs L., Randles C. A.,  
502 Darnenov A., Bosilovich M. G., Reichle R., Wargan K., Coy L., Cullather R., Draper C., Akella S.,  
503 Buchard V., Conaty A., Silva A. M. d., Gu W., Kim G.-K., Koster R., Lucchesi R., Merkova D., Nielsen  
504 J. E., Partyka G., Pawson S., Putman W., Rienecker M., Schubert S. D., Sienkiewicz M. & Zhao B.: The  
505 Modern-Era Retrospective Analysis for Research and Applications, Version 2 (MERRA-2), *Journal of*  
506 *Climate.* 30(14), 5419-5454, 10.1175/jcli-d-16-0758.1, 2017.



- 507 Giorgi F., Coppola, E., Solmon, F., Mariotti, L., Sylla, M.B., Bi, X., Elguindi, N., Diro, G.T.,  
508 Nair, V., Giuliani, G., Turuncoglu, U.U., Cozzini, S., Güttler, I., O'Brien, T.A., Shalaby A. Tawfik, A.  
509 B., Zakey, A.S., Steiner, A.L., Stordal, F., Sloan, L.C., & Brankovic C.: RegCM4: model description  
510 and preliminary tests over multiple CORDEX domains. *Clim. Res.*, 52:7–29. doi: 10.3354/cr01018,  
511 2012.
- 512 Grabe, F.: Simulation der Wechselwirkung zwischen Atmosphäre, Vegetation und  
513 Erdoberfläche bei Verwendung unterschiedlicher Parametrisierungsansätze. PhD Thesis. Inst. for  
514 Meteorology and Climate Research, Karlsruhe Institute of Technology, Karlsruhe, Germany, 2002.
- 515 Grünewald, T., Bühler, Y., and Lehning, M.: Elevation dependency of mountain snow depth,  
516 *The Cryosphere*, 8, 2381–2394, <https://doi.org/10.5194/tc-8-2381-2014>, 2014.
- 517 Gobiet, A., Kotlarski, S., Beniston, M., Heinrich, G., Rajczak, J., Stoffel, M.: 21st century  
518 climate change in the European Alps—A review. *Science of the Total Environment* 493, 1138–1151,  
519 2014.
- 520 Henderson, G. R., Peings, Y., Furtado, J. C. & Kushner, P. J.: Snow–atmosphere coupling in  
521 the Northern Hemisphere, *Nature Climate Change*. 8(11), 954-963, 10.1038/s41558-018-0295-6, 2018.
- 522 Hall, D. K. and Riggs, G.A.: MODIS/Terra Snow Cover Daily L3 Global 0.05Deg CMG,  
523 Version 6. Boulder, Colorado USA. NASA National Snow and Ice Data Center Distributed Active  
524 Archive Center. doi: <https://doi.org/10.5067/MODIS/MOD10C1.006>. (accessed on 15.08.2020), 2016.
- 525 Jacob, D., and Coauthors: Assessing the transferability of the regional climate model REMO to  
526 different CORDEX regions, *Atmosphere*, 3, 181-199, DOI:10.3390/atmos3010181, 2012.
- 527 Jonas, T., and Essery R.: Snow Cover and Snowmelt in Forest Regions. In: Singh V.P., Singh  
528 P., Haritashya U.K. (eds) *Encyclopedia of Snow, Ice and Glaciers*. *Encyclopedia of Earth Sciences*  
529 *Series*. Springer, Dordrecht. [https://doi.org/10.1007/978-90-481-2642-2\\_499](https://doi.org/10.1007/978-90-481-2642-2_499), 2014.
- 530 Jacob, D., Petersen, J., Eggert, B., Alias, A., Christensen, O. B., Bouwer, L. M., Braun, A.,  
531 Colette, A., Déqué, M., Georgievski, G., Georgopoulou, E., Gobiet, A., Menut, L., Nikulin, G., Haensler,  
532 A., Hempelmann, N., Jones, C., Keuler, K., Kovats, S., Kröner, N., Kotlarski, S., Kriegsmann, A.,  
533 Martin, E., van Meijgaard, E., Moseley, C., Pfeifer, S., Preuschmann, S., Radermacher, C., Radtke, K.,  
534 Rechid, D., Rounsevell, M., Samuelsson, P., Somot, S., Soussana, J.-F., Teichmann, C., Valentini, R.,



- 535 Vautard, R., Weber, B. & Yiou, P.: EURO-CORDEX: new high-resolution climate change projections  
536 for European impact research, *Regional Environmental Change*. 14(2), 563-578, 10.1007/s10113-013-  
537 0499-2, 2014.
- 538 Jacob, D., Teichmann, C., Sobolowski, S. et al.: Regional climate downscaling over Europe:  
539 perspectives from the EURO-CORDEX community. *Reg Environ Change* **20**, 51.  
540 <https://doi.org/10.1007/s10113-020-01606-9>, 2020.
- 541 Kotlarski, S.: A Subgrid Glacier Parameterisation for Use in Regional Climate Modelling, Max-  
542 Planck Institut für Meteorologie Report No. \*\*, 2007.
- 543 Lawrence, D. & Coauthors: Technical Description of version 5.0 of the Community Land Model  
544 (CLM), Boulder, CO, 329 pp, 2020.
- 545 Lüthi, S., Ban, N., Kotlarski, S., Steger, C.R., Jonas, T., Schär, C.: Projections of Alpine Snow-  
546 Cover in a High-Resolution Climate Simulation. *Atmosphere.*; 10(8):463.  
547 <https://doi.org/10.3390/atmos10080463>, 2019.
- 548 Magnusson, J., Tobias, J., López-Moreno, I., Lehning, M.; Snow cover response to climate  
549 change in a high alpine and half-glacierized basin in Switzerland. *Hydrology Research*; 41 (3-4): 230–  
550 240. doi: <https://doi.org/10.2166/nh.2010.115>, 2010.
- 551 Matiu, M., Petitta, M., Notarnicola, C., Zebisch, M. Evaluating Snow in EURO-CORDEX  
552 Regional Climate Models with Observations for the European Alps: Biases and Their Relationship to  
553 Orography, Temperature, and Precipitation Mismatches. *Atmosphere.* 11(1):46.  
554 <https://doi.org/10.3390/atmos11010046>, 2020.
- 555 Matiu, M., Crespi, A., Bertoldi, G., Carmagnola, C. M., Marty, C., Morin, S., Schöner, W., Cat  
556 Berro, D., Chiogna, G., De Gregorio, L., Kotlarski, S., Majone, B., Resch, G., Terzago, S., Valt, M.,  
557 Beozzo, W., Cianfarra, P., Gouttevin, I., Marcolini, G., Notarnicola, C., Petitta, M., Scherrer, S. C.,  
558 Strasser, U., Winkler, M., Zebisch, M., Cicogna, A., Cremonini, R., Debernardi, A., Faletto, M., Gaddo,  
559 M., Giovannini, L., Mercalli, L., Soubeyroux, J.-M., Sušnik, A., Trenti, A., Urbani, S., and Weilguni,  
560 V.: Observed snow depth trends in the European Alps: 1971 to 2019, *The Cryosphere*, 15, 1343–1382,  
561 <https://doi.org/10.5194/tc-15-1343-2021>, 2021.



- 562 Mioduszewski, J.R., Rennermalm, A.K., Robinson, D.A., Wang, L. Controls on spatial and  
563 temporal variability in Northern Hemisphere terrestrial snowmelt timing, 1979-2012. *Journal of*  
564 *Climate*, 28 (6), pp. 2136-2153, 2015.
- 565 Moeser, D., Mazzotti, G., Helbig, N., and Jonas, T.: Representing spatial variability of forest  
566 snow: Implementation of a new interception model, *Water Resour. Res.*, 52, 1208– 1226,  
567 doi:10.1002/2015WR017961, 2016.
- 568 Mooney, P. A., Lee, H., and Sobolowski, S.: Impact of quasi-idealized future land cover  
569 scenarios at high latitudes in complex terrain. *Earth's Future*, 9 (2), e2020EF001838.  
570 <https://doi.org/10.1029/2020EF001838>, 2021.
- 571 Muñoz Sabater, J.: ERA5-Land monthly averaged data from 1981 to present. Copernicus  
572 Climate Change Service (C3S) Climate Data Store (CDS). (accessed on 31.08.2020),  
573 10.24381/cds.68d2bb30, 2019.
- 574 Muñoz-Sabater, J., Dutra, E., Agustí-Panareda, A., Albergel, C., Arduini, G., Balsamo, G.,  
575 Boussetta, S., Choulga, M., Harrigan, S., Hersbach, H., Martens, B., Miralles, D. G., Piles, M.,  
576 Rodríguez-Fernández, N. J., Zsoter, E., Buontempo, C., and Thépaut, J.-N.: ERA5-Land: A state-of-the-  
577 art global reanalysis dataset for land applications, *Earth Syst. Sci. Data Discuss.* [preprint],  
578 <https://doi.org/10.5194/essd-2021-82>, in review, 2021.
- 579 Niu, G.-Y., and Yang, Z.L.: The effects of canopy processes on snow surface energy and mass  
580 balances, *J. Geophys. Res.*, 109, D23111, doi:10.1029/2004JD004884, 2004.
- 581 Niu, G.-Y., and Z.-L. Yang: An observation-based formulation of snow cover fraction and its  
582 evaluation over large North American river basins, *J. Geophys. Res.*, 112, D21101,  
583 doi:10.1029/2007JD008674, 2007.
- 584 Niu, G. Y., & Coauthors: The community Noah land surface model with multiparameterization  
585 options (Noah-MP): 1. Model description and evaluation with local-scale measurements. *Journal of*  
586 *Geophysical Research: Atmospheres*, 116(D12), 2011.
- 587 Oleson, K. W., Lawrence, D. M., Bonan, G. B., Flanner, M. G., Kluzek, E., Lawrence, P. J., ...  
588 Zeng, X.: Technical Description of version 4.0 of the Community Land Model (CLM) (No. NCAR/TN-  
589 478+STR). University Corporation for Atmospheric Research. doi:10.5065/D6FB50WZ, 2010.



590 Oleson K. W. & Coauthors: Technical description of version 4.5 of the Community Land Model  
591 (CLM). Boulder, CO, 420 pp, 2013.

592 Pomeroy, J.W., Gray, D.M., Shook, K.R., Toth, B., Essery, R.L.H., Pietroniro, A. and  
593 Hedstrom, N.: An evaluation of snow accumulation and ablation processes for land surface modelling.  
594 Hydrol. Process., 12: 2339-2367. [https://doi.org/10.1002/\(SICI\)1099-1085\(199812\)12:15<2339::AID-](https://doi.org/10.1002/(SICI)1099-1085(199812)12:15<2339::AID-HYP800>3.0.CO;2-L)  
595 [HYP800>3.0.CO;2-L](https://doi.org/10.1002/(SICI)1099-1085(199812)12:15<2339::AID-HYP800>3.0.CO;2-L), 1998.

596 Thackeray, C.W., Qu, X. and Hall, A.: Why do models produce spread in snow albedo  
597 feedback?. Geophysical Research Letters, 45(12), pp.6223-6231, 2018.

598 Qu, X., and A. Hall: What Controls the Strength of Snow-Albedo Feedback?. *J. Climate*, **20**,  
599 3971–3981, <https://doi.org/10.1175/JCLI4186.1>, 2007.

600 Qu X. and A. Hall: On the persistent spread in snow-albedo feedback. *Clim Dyn*, 42:69–81  
601 DOI:10.1007/s00382-013-1774-0, 2014.

602 Reinhart V., Fonte C., Hoffmann P., Bechtel B., Rechid D., Böhner J.: Comparison of ESA  
603 Climate Change Initiative Land Cover to CORINE Land Cover over Eastern Europe and the Baltic  
604 States from a regional climate modeling perspective. *Int. J. Earth Obs.* 94, 102221.  
605 <https://doi.org/10.1016/j.jag.2020.102221>, 2020.

606 Rechid, D., Davin, E., de Noblet-Ducoudré, N., and Katragkou, E.: CORDEX Flagship Pilot  
607 Study LUCAS – Land Use & Climate Across Scales – a new initiative on coordinated regional land use  
608 change and climate experiments for Europe, in 19th EGU General Assembly, EGU2017, proceedings  
609 from the conference held 23–28 April, 2017 in Vienna, Austria, 19, p. 13172, 2017.

610 Rockel B., Will A. & Hense A.: The regional climate model COSMO-CLM (CCLM).  
611 *Meteorologische Zeitschrift*, 17(4), 347-348, 2008.

612 Roeckner E., Arpe K., Bentsson L., Christoph M., Claussen M., Dümenil L., Esch M., Giorgetta  
613 M., Schlese U. & Schulzweida U.: The atmospheric general circulation model ECHAM-4: Model  
614 description and simulation of present day climate. Max-Planck Institut für Meteorologie Report No. 218,  
615 90 pp. , 1996.



616 Samuelsson, P., Gollvik S., Jansson, C., Kupiainen, M., Kourzeneva, E., & Jan van de Berg,  
617 W.: The surface processes of the Rossby Centre regional atmospheric climate model (RCA4). Reports  
618 METEOROLOGY, 157, SMHI, Norrköping, Sweden, 2015.

619 Samuelsson, P., Gollvik, S., & Ullerstig, A.: The land-surface scheme of the Rossby Centre  
620 regional atmospheric model (RCA3). Reports Meteorology, 122, SMHI, SE-60176 Norrköping,  
621 Sweden, 2006.

622 Schrodin, E., and Heise, E.: A new multi-layer soil model. COSMO Newsletter No. 2:149-151,  
623 2002.

624 Skamarock, W. C., and Coauthors: A description of the advanced research WRF version 3,  
625 NCAR Technical Note. *National Center for Atmospheric Research, Boulder, Colorado, USA*, 2008.

626 Sofiadis, G., Katragkou, E., Davin, E. L., Rechid, D., de Noblet-Ducoudre, N., Breil, M.,  
627 Cardoso, R. M., Hoffmann, P., Jach, L., Meier, R., Mooney, P., Soares, P. M. M., Strada, S., Tolle, M.  
628 H., and Warrach Sagi, K.: Afforestation impact on soil temperature in regional climate model  
629 simulations over Europe, Geosci. Model Dev. Discuss. [preprint], [https://doi.org/10.5194/gmd-2021-](https://doi.org/10.5194/gmd-2021-69)  
630 69, in review, 2021.

631 Strandberg, G., Bärring L., Hansson U., Jansson C., Jones C., Kjellström E., Kolax M.,  
632 Kupiainen M., Nikulin G., Samuelsson P., Ullerstig A. & Wang S.: CORDEX scenarios for Europe  
633 from the Rossby Centre regional climate model RCA4. SMHI Meteorology and Climatology Rep. 116,  
634 84 pp.,  
635 [https://www.smhi.se/polopoly\\_fs/1.90275!/Menu/general/extGroup/attachmentColHold/mainColl1/file](https://www.smhi.se/polopoly_fs/1.90275!/Menu/general/extGroup/attachmentColHold/mainColl1/file/RMK_116.pdf)  
636 [/RMK\\_116.pdf](https://www.smhi.se/polopoly_fs/1.90275!/Menu/general/extGroup/attachmentColHold/mainColl1/file/RMK_116.pdf), 2015.

637 Sørland, S. L., Brogli, R., Pothapakula, P. K., Russo, E., Van de Walle, J., Ahrens, B., Anders,  
638 I., Buchignani, E., Davin, E. L., Demory, M.-E., Dosio, A., Feldmann, H., Früh, B., Geyer, B., Keuler,  
639 K., Lee, D., Li, D., van Lipzig, N. P. M., Min, S.-K., Paniz, H.-J., Rockel, B., Schär, C., Steger, C., and  
640 Thiery, W.: COSMO-CLM Regional Climate Simulations in the CORDEX framework: a review,  
641 Geosci. Model Dev. Discuss. [preprint], <https://doi.org/10.5194/gmd-2020-443>, in review, 2021.

642 van Kampenhout, L., J.T.M. Lenaerts, W.H. Lipscomb, W.J. Sacks, D.M. Lawrence, A.G. Slater  
643 & M.R. van den Broeke: Improving the Representation of Polar Snow and Firn in the Community Earth





644 System Model. *Journal of Advances in Modeling Earth Systems* 9, no. 7: 2583–2600.  
645 <https://doi.org/10.1002/2017MS000988>, 2017.

646 Wang A. & Zeng X.: Improving the treatment of the vertical snow burial fraction over short  
647 vegetation in the NCAR CLM3, *Advances in Atmospheric Sciences*. 26(5), 877-886, 10.1007/s00376-  
648 009-8098-3, 2009.

649 Wilhelm C., Rechid D. & D. Jacob: Interactive coupling of regional atmosphere with biosphere  
650 in the new generation regional climate system model REMO-iMOVE. *Geoscientific Model  
651 Development*, 7(3), 1093-1114, 2014.

652 Xu, L., & Dirmeyer, P.: Snow–Atmosphere Coupling Strength. Part I: Effect of Model Biases,  
653 *Journal of Hydrometeorology*. 14(2), 389-403, 10.1175/jhm-d-11-0102.1, 2013.

654 Xu, L., and Dirmeyer, P.: Snow-atmosphere coupling strength in a global atmospheric model,  
655 *Geophys. Res. Lett.*, 38, L13401, doi:10.1029/2011GL048049, 2011.

656 Ye, H. and Cohen, J.: A shorter snowfall season associated with higher air temperatures over  
657 northern Eurasia, *Environmental Research Letters*, 8, 014052, doi:10.1088/1748-9326/8/1/014052,  
658 2013.

659

660

661

662

663

664

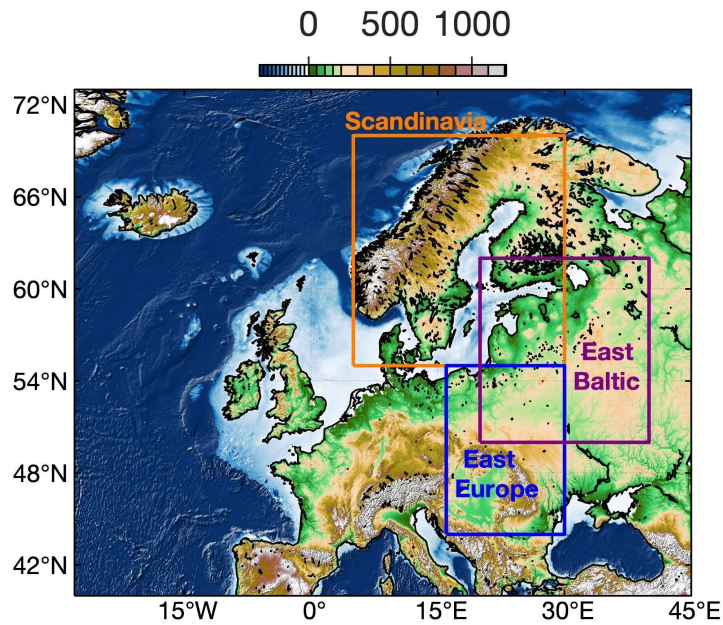
665

666

667



668 **Figures and Tables**

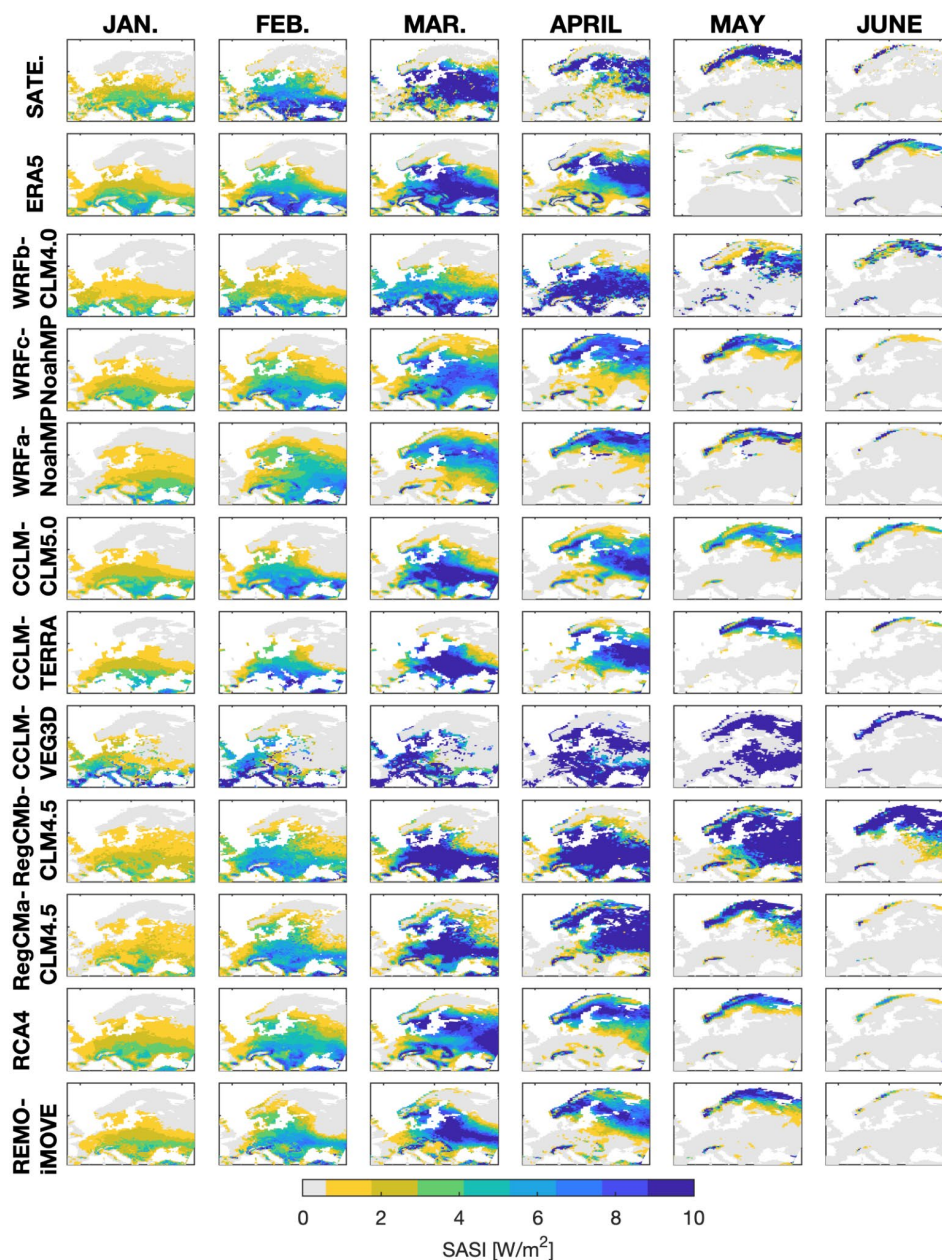


669

670 **Figure 1:** Map showing the location of the three regions of interest: Scandinavia (red), East Baltic (pink)

671 and East Europe (blue).

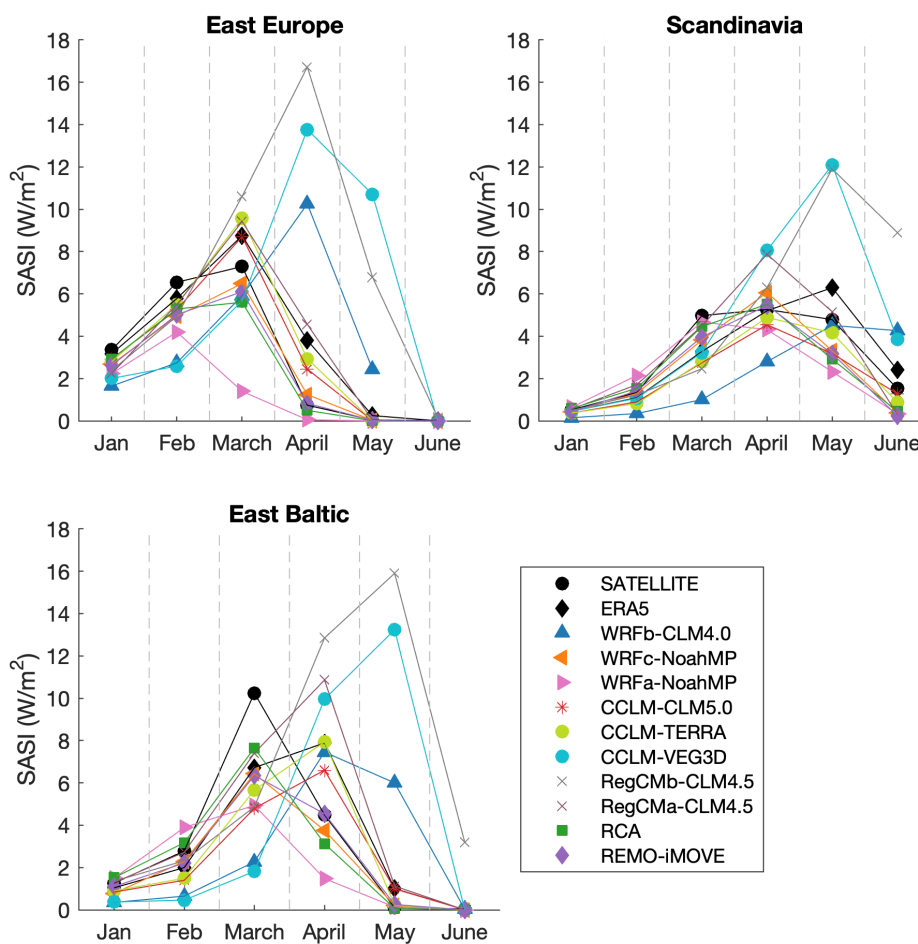
672



673

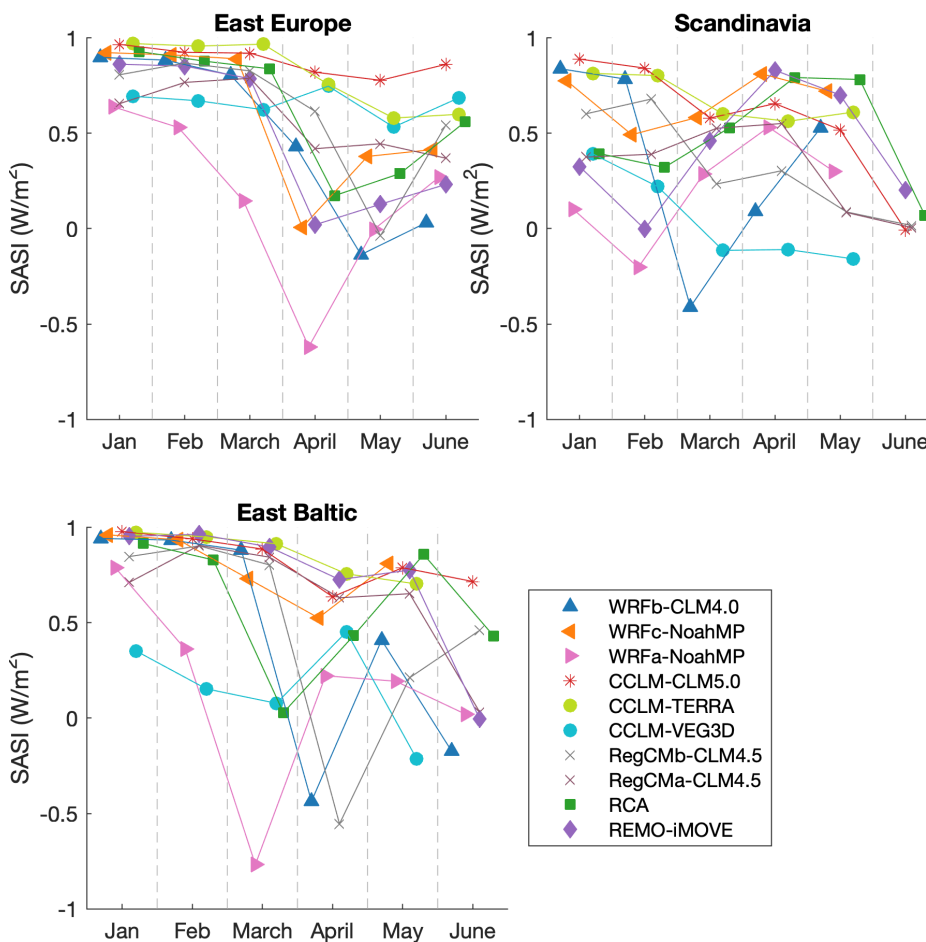
674 **Figure 2:** Spatial maps of SASI ( $\text{Wm}^{-2}$ ) for satellite observations, the reanalysis ERA5-Land and the  
675 ten regional climate simulations from the EVAL experiment of LUCAS from January to June, averaged  
676 over the time period 1986-2015.

677



678

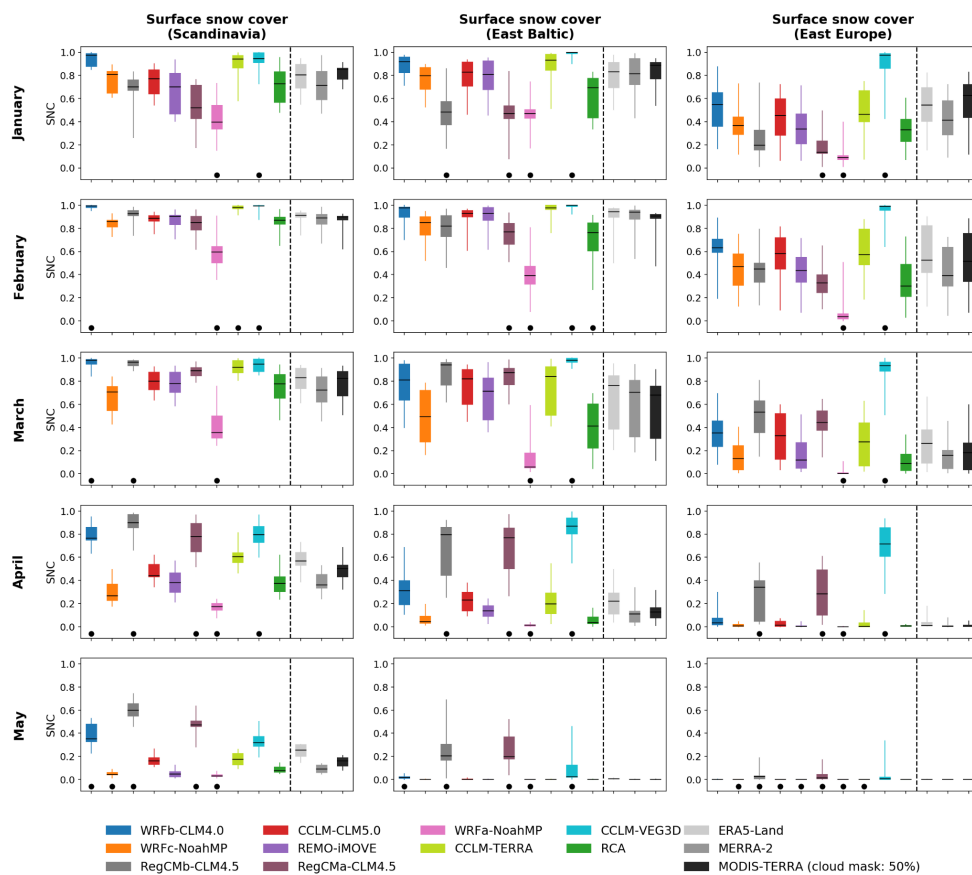
679 **Figure 3:** Time series of the spatial average of SASI for the satellite observations, the reanalysis ERA5-  
 680 Land and the ten regional climate simulations from the EVAL experiment of LUCAS in Scandinavia,  
 681 East Europe and East Baltic (see Figure 1 for their spatial extent). Data are averaged over the time period  
 682 1986-2015.



683

684 **Figure 4:** As in Figure 3 but for the pattern correlation between SASI and ERA5-Land for the LUCAS

685 simulations.

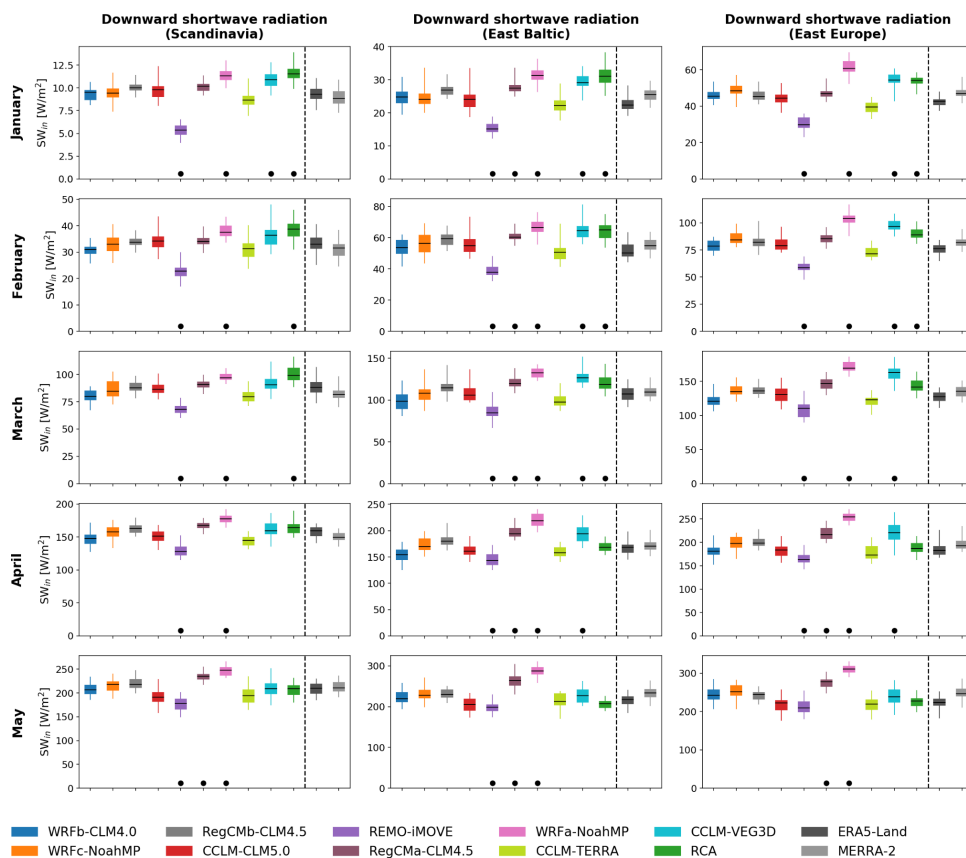


686

687 **Figure 5:** Snow cover for the 10 RCMs, MERRA-2, ERA5-Land, and MODIS satellite observations  
 688 (using only data from days and pixels with less than 50% cloud cover) for January to May. The box-  
 689 and-whisker-plots show the interannual variability of snow cover over 1986-2015, with the bar  
 690 representing the median, boxes the interquartile range, and whiskers the minimum/maximum values.  
 691 Dots indicate models lying outside the range of the reference datasets MERRA-2, ERA5-Land, and  
 692 MODIS (i.e., the 25th (75th) model percentile is higher (lower) than the highest 75th (lowest 25th)  
 693 quantile of the reference datasets).

694

695

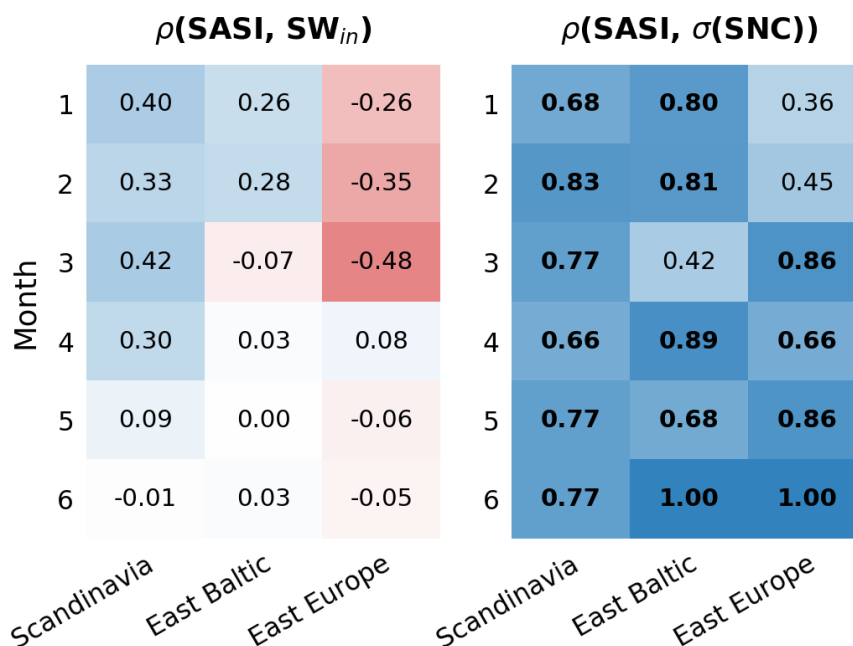


696

697 **Figure 6:** Downward surface shortwave radiation for the 10 RCMs for MERRA-2, and ERA5-Land, for  
 698 January to May. The box-and-whisker-plots show the interannual variability of downward shortwave  
 699 radiation over 1986-2015, with the bar representing the median, boxes the interquartile range, and  
 700 whiskers the minimum/maximum values. Dots indicate models lying outside the range of the reference  
 701 datasets MERRA-2, ERA5-Land, and MODIS (i.e., the 25th (75th) model percentile is higher (lower)  
 702 than the highest 75th (lowest 25th) quantile of the reference datasets).

703





704

705 **Figure 7:** Pearson correlation between SASI and shortwave radiation (left), and SASI and standard  
 706 deviation of snow cover (right) calculated across RCMs for the three regions Scandinavia, East Baltic,  
 707 and East Europe for the months January to June during 1986-2015. The values represent the variable  
 708 (shortwave radiation or variability in snow cover) to which the inter-model variability of SASI is  
 709 predominantly related to. Bold values indicate statistical significance at the 0.05 level (two-tailed p-  
 710 value).

711

712

713

714

715

716

717





Institute ID	RCM	LSM	Representation of sub-grid scale surface heterogeneity	Phenology	Snow- vegetation interaction	Name of the models
<b>BCCR</b>	WRF v3.8.1 [Skamarock et al., 2008]	NoahMP [Niu et al., 2011]	PFT-dominant	Prescribed	Deardorff, 1978; Niu and Yang, 2007	WRFc-NoahMP
<b>CUNI</b>	RegCM v4.7 [Giorgi et al., 2012]	CLM4.5 [Oleson et al., 2013]	PFT-tile	Prescribed	Wang and Zeng, 2009	RegCMb-CLM4.5
<b>ETH</b>	Cosmo_5.0_clm9 [Soerland et al., 2021]	CLM5.0 [Lawrence et al., 2020]	PFT-tile	Prescribed	Wang and Zeng, 2009; Lawrence et al., 2020; van Kampenhout et al., 2017	CCLM-CLM5.0
<b>GERICS</b>	REMO2009 [Jacob et al., 2012]	iMOVE [Wilhelm et al., 2014]	PFT-tile	Interactive	Roeckner et al., 1996; Kotlarski, 2007	REMO-iMOVE
<b>ICTP</b>	RegCM v4.6 [Giorgi et al., 2012]	CLM4.5 [Oleson et al., 2013]	PFT-tile	Prescribed	Wang and Zeng, 2009	RegCMa-CLM4.5
<b>IDL</b>	WRF v3.8.1D [Skamarock et al., 2008]	NoahMP [Niu et al., 2011]	PFT-dominant	Prescribed	Deardorff, 1978; Niu and Yang, 2007	WRFa-NoahMP
<b>KIT</b>	Cosmo_5.0_clm9 [Soerland et al., 2021; Rockel et al., 2008]	VEG3D [Braun and Schädler, 2005]	PFT-dominant	Prescribed	Grabe, 2002	CCLM-VEG3D
<b>SMHI</b>	RCA4 [Strandberg et al., 2015]	Internal [Samuelsson et al., 2006]	PFT-tile	Prescribed	Samuelsson et al., 2015	RCA
<b>AUTH</b>	WRF v3.8.1 [Skamarock et al., 2008]	CLM4.0 [Oleson et al., 2010]	PFT-tile	Prescribed	Wang and Zeng, 2009	WRFb-CLM4.0
<b>CLMcom-JLU</b>	Cosmo_5.0_clm9 [Soerland et al., 2021]	TERRA-ML [Schrodin and Heise, 2002]	PFT-dominant	Prescribed	Doms et al., 2013	CCLM-TERRA

718 **Table 1:** Summary of participating RCMs and their LSMs.

719